Achilles' heel of a traveling pulse subject to a local external stimulus

Kei Nishi,[1,*] Shogo Suzuki,[2] Katsuhiko Kayahara,[2] Masakazu Kuze,[2] Hiroyuki Kitahata,[3]
Satoshi Nakata,[2,†] and Yasumasa Nishiura[4,‡]

[1]*Department of Mathematics, Graduate School of Science, Kyoto Sangyo University, Kyoto 603-8555, Japan*
[2]*Department of Mathematical and Life Sciences, Graduate School of Science, Hiroshima University, Higashi-Hiroshima 739-8526, Japan*
[3]*Department of Physics, Chiba University, Chiba 263-8522, Japan*
[4]*Advanced Institute for Materials Research (WPI-AIMR), Tohoku University, Sendai 980-8577, Japan*

(Received 9 March 2017; published 12 June 2017)

The response of a traveling pulse to a local external stimulus is considered numerically for a modified three-component Oregonator, which is a model system for the photosensitive Belousov-Zhabotinsky (BZ) reaction. The traveling pulse is traced and constantly stimulated, with the distance between the pulse and the stimulus being kept constant. We are interested in the minimal strength of the spatially localized stimulus in order to eliminate the pulse. The use of a stimulus of small width allows us to detect the point in the pulse most sensitive to the external stimulus, referred to as the "Achilles' heel" of the traveling pulse, at which minimal strength of stimulus causes a collapse of the pulse. Our findings are demonstrated experimentally as well with the photosensitive BZ reaction.

DOI: 10.1103/PhysRevE.95.062209

I. INTRODUCTION

The traveling wave is one of the most ubiquitous patterns observed in extended dissipative systems, including heart tissues [1,2], nerve axons [3,4], retinas [5,6], social amoebae [7,8], gas discharge devices [9,10], and oxidization reactions on Pt surfaces [11]. Such wave patterns in different spatial dimensions, i.e., traveling pulses in one spatial dimension, concentric and spiral waves in two spatial dimensions, and scroll waves in three spatial dimensions, have been analyzed extensively for reaction-diffusion systems [12,13]. In order to make the analysis tractable, the homogeneity of the system is typically assumed. However, pattern formation in nature proceeds in inherently heterogeneous environments. Over the past few decades, therefore, a number of experiments have been conducted to investigate the influence of spatiotemporal heterogeneity on the dynamics of traveling patterns [14–25].

One experimental system suitable for examining the effect of heterogeneity is the photosensitive Belousov-Zhabotinsky (BZ) reaction [26,27], in which light irradiation results in the production of bromide, changing the reaction rate according to the local intensity of the irradiation. This property allows us to realize any type of heterogeneity or domain shape by appropriately changing the intensity of light irradiation and the form of the irradiated region. In fact, various types of heterogeneity have been designed for the photosensitive BZ media to investigate the dynamics of propagating waves under the influence of heterogeneity, in which preservation [28], splitting [29], initiation [30,31], propagation failure [32–34], and wave emission [35] were observed. Analytical studies were also performed simultaneously to clarify the underlying mechanisms for the heterogeneity-induced spatiotemporal behaviors [36–41].

On the other hand, the fact that heterogeneity induces a variety of dynamics means that it can potentially be utilized for controlling patterns. In fact, the spontaneous and flexible responses of traveling waves to external stimuli and environmental changes were applied not only to controlling the direction of chemical wave propagation [42–46] and droplet motion [47], but also to the construction of chemical information processing devices [48–50], to optimal path finding [51], and to defibrillation in beating hearts [52,53]. External stimuli of lower energy and reduced cost would be desirable for the control of patterns, particularly in application to living systems. However, there is a considerable lack of effort for seeking efficient and less destructive ways of controlling patterns.

In our previous study [54], the response of a traveling pulse to a stimulus localized in both space and time was investigated experimentally and numerically for the photosensitive BZ medium by irradiating the pulse locally for a certain period of time. The experiments not only revealed the dependence of the propagation velocity on the onset time of the light irradiation, but also suggested the existence of a sensitive point of the traveling pulse to the local stimulus. However, the most vulnerable part of the pulse is not easily identifiable, since the irradiated region was fixed in space while the pulse kept moving. Furthermore, our previous study was only concerned with a relatively low intensity regime to study the propagation velocity [54].

In this paper, we study the behavior of a traveling pulse, both numerically and experimentally, under a comoving local stimulus that is strong enough to make the pulse disappear. The region of the stimulus was moved along with the traveling pulse such that the pulse is continuously exposed to the stimulus at a fixed point. Our main objective here is twofold. First, we examine whether an extremely narrow stimulus can cause a collapse of the pulse. It is well known that the pulse collapses under a strong irradiation for the experiment on the photosensitive BZ reaction when the irradiated region is large enough to cover the target pattern [32]. Instead, we employ a local irradiation of small width and relatively high intensity to examine whether the pulse collapses with a sufficiently small irradiation width. Next, even for the same shape and size of the stimulus, the strength of the stimulus required to make the

*Corresponding author: knishi@cc.kyoto-su.ac.jp
†Corresponding author: nakatas@hiroshima-u.ac.jp
‡Corresponding author: yasumasa.nishiura.a6@tohoku.ac.jp

pulse collapse would also differ according to the part of the pulse being stimulated due to the extended spatial structure of the traveling pulse. In particular, some part of the pulse may be sensitive to the external stimulus, as suggested by our previous results [54]. We call such a sensitive point of the traveling pulse, if it exists, an "Achilles' heel" throughout the paper. If such a special point is identified, we may be able to efficiently eliminate the traveling pulse by providing a local stimulus to the special point.

The paper is organized as follows. In Sec. II, the setting for our problem is introduced, along with the model reaction-diffusion equations with modified three-component Oregonator kinetics. In Sec. III, the behavior of the traveling wave under the local irradiation is investigated numerically for the model equations. In Sec. IV, experiments corresponding to the numerical study are performed using a photosensitive BZ medium. The location of an "Achilles' heel" is further discussed in Sec. V.

II. MODEL SYSTEM

Several model systems have been proposed to describe the pattern formation in photosensitive BZ reactions. One of the most frequently utilized systems is a reaction-diffusion system with its local dynamics governed by the modified Oregonator. Throughout this paper, we employ the following three-component reaction-diffusion system with Oregonator kinetics that allows for photosensitivity [33,42,44,50,55]:

$$\begin{aligned}\frac{\partial u}{\partial t} &= D_u\frac{\partial^2 u}{\partial x^2} + \frac{1}{\epsilon_1}(u - u^2 + qw - uw),\\ \frac{\partial v}{\partial t} &= D_v\frac{\partial^2 v}{\partial x^2} + u - v,\\ \frac{\partial w}{\partial t} &= D_w\frac{\partial^2 w}{\partial x^2} + \frac{1}{\epsilon_2}(\phi(x,t) - qw - uw + fv),\end{aligned} \tag{1}$$

where $u(x,t)$, $v(x,t)$, and $w(x,t)$ $(x \in \mathbf{R}, t > 0)$ are dimensionless variables that correspond to the concentrations of the activator $HBrO_2$, the oxidized catalyst $Ru(bpy)_3^{3+}$, and the inhibitor Br^-, respectively. It can be noted that light emission from the photosensitive catalyst $Ru(bpy)_3^{3+}$ is usually measured in actual experiments. The effect of light irradiation is reflected in the function $\phi(x,t)$ that takes arbitrary forms depending on the situation of concern. As we shall see in the next section, in the case of $\phi(x,t) \equiv \phi_0$, a stable traveling pulse solution is numerically found for (1) when the parameters are chosen as $\epsilon_1 = 0.050\,8$, $\epsilon_2 = 0.000\,168$, $q = 0.000\,1$, $f = 2.5$, $D_u = D_v = D_w = 1.0$, and $\phi_0 = 0.000\,5$ [42,50,54]. Note that the kinetics is of excitable type for the above parameter set. In this paper, we consider the situation where a specific part of the traveling pulse is continuously irradiated by moving a finite-width irradiation region along with the pulse [Fig. 1(a)].

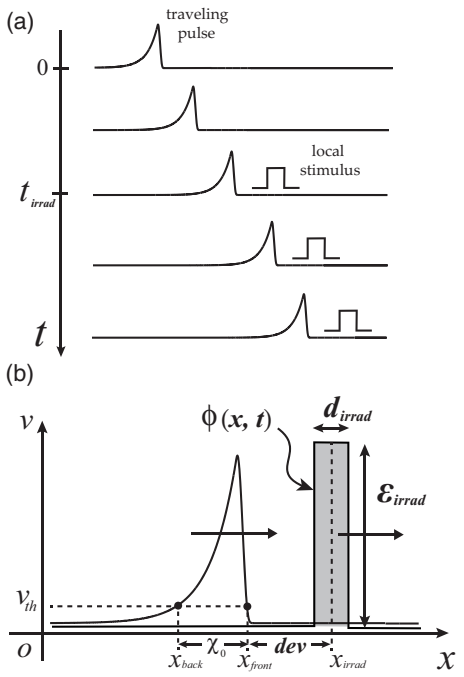

FIG. 1. Schematic figures for our problem setting. (a) A stable traveling pulse is stimulated for $t \geqslant t_{\rm irrad}$ with a local light irradiation that moves together with the pulse. (b) The irradiation function $\phi(x,t)$ is changed so that the distance dev between the pulse front $x_{\rm front}$ and the irradiation center $x_{\rm irrad}$ is kept constant. Here, the pulse front and the pulse back are defined as the intersections of the v component $v(x,t)$ of a traveling pulse solution with some fixed threshold v_{th}. The pulse width $\chi_0(t)$ is also defined as $\chi_0(t) = x_{\rm front}(t) - x_{\rm back}(t)$. During the irradiation, the width $d_{\rm irrad}$ and the intensity $\epsilon_{\rm irrad}$ are fixed.

More specifically, the irradiation $\phi(x,t)$ is determined according to the following procedure: In order to keep track of the traveling pulse, its position should be defined. Therefore we first take some small value v_{th} as a threshold, which is to be fixed throughout the irradiation. Here, we take it to be $1/10$ of the maximal value $v_{\max}$ of the variable $v(x,t)$ of the stable traveling pulse solution for $\phi(x,t) \equiv \phi_0$ (i.e., $v_{th} = v_{\max}/10$). Then the pulse front $x_{\rm front}(t)$, as well as the pulse back $x_{\rm back}(t)$, is defined as the intersection of $v(x,t)$ with the threshold v_{th} (i.e., $v\,[x_{\rm front}(t),t\,] = v\,[x_{\rm back}(t),t\,] = v_{th}$). Note that the aforementioned definition of interfaces does not work well for the two-component Oregonator system [32,35], which is why we adopt the three-component system. Now that the pulse front is defined, let us proceed to the form of the irradiation $\phi(x,t)$. We apply a local irradiation of width $d_{\rm irrad}$ and intensity $\epsilon_{\rm irrad}$ centered at $x = x_{\rm irrad}(t)$, which is switched on at some time $t = t_{\rm irrad}$. Also, a parameter dev is defined as the distance between the position of the pulse front and the center of the irradiation [i.e., $dev = x_{\rm irrad}(t) - x_{\rm front}(t)$, Fig. 1(b)]. Summarizing the above, the function $\phi(x,t)$ is explicitly written as

$$\phi(x,t) = \begin{cases}\phi_0 & (0 < t < t_{\rm irrad}),\\ \phi_0 + \epsilon_{\rm irrad}\,H(d_{\rm irrad}/2 - |x - x_{\rm irrad}(t)|) & (t \geqslant t_{\rm irrad}),\end{cases} \tag{2}$$

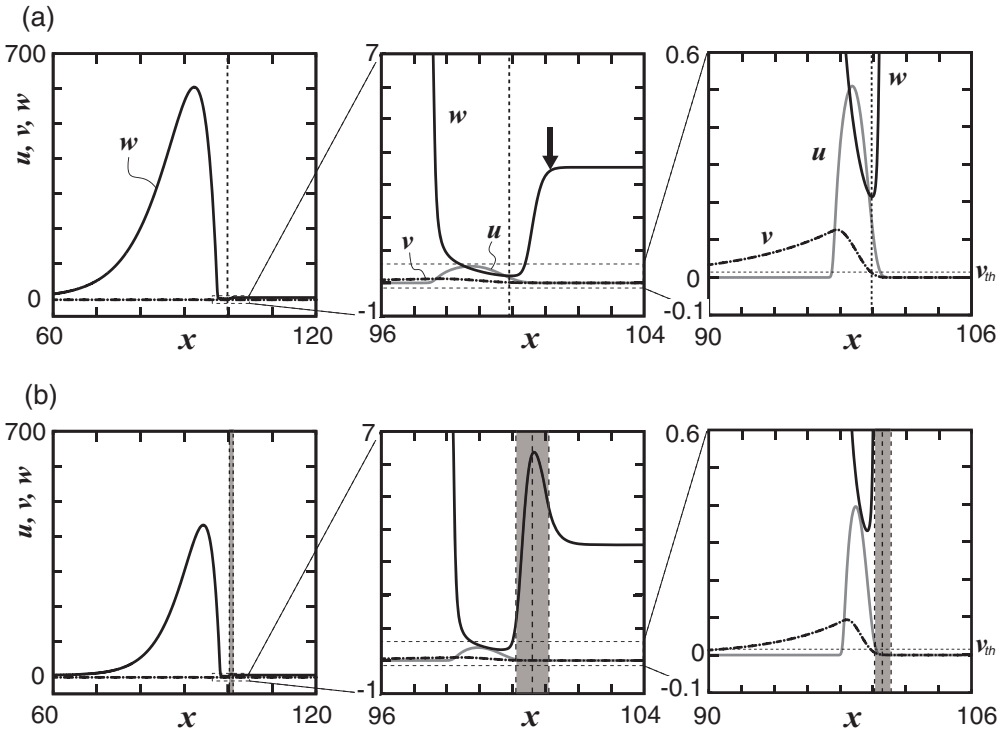

FIG. 2. The profile of a stable rightward-traveling pulse solution observed numerically in (1) with (2) for (a) $\epsilon_{\text{irrad}} = 0$ and (b) $\epsilon_{\text{irrad}} \neq 0$. The figures in the middle and on the right are magnifications of those on the left. The u, v, and w components are represented by the gray solid, dot-dash, and black solid curves, respectively. (a) Before the irradiation, the maximal value $v_{\max}$ of the v component is about 0.127 4, such that the threshold v_{th} for determining the pulse front is fixed as $v_{th} = 0.012\,74$. The dashed vertical lines denote the position of the pulse front x_{front}, defined as $v[\,x_{\text{front}}(t), t\,] = v_{th}$. In the middle figure, the edge of the dent in the w component is indicated by the bold arrow. (b) Under the irradiation, the size of the irradiated traveling pulse (ITP) becomes smaller than that from before the irradiation in (a). The parameters for the irradiation in (2) are fixed as $d_{\text{irrad}} = 1.0$, $dev = 0.6$, and $\epsilon_{\text{irrad}} = 0.004\,53$. The irradiated part is indicated by the shaded regions. In (a) and (b), the numerical simulation is performed for $x \in [0,200)$ with the periodic boundary condition, and the other parameters are chosen as $\epsilon_1 = 0.050\,8$, $\epsilon_2 = 0.000\,168$, $q = 0.000\,1$, $f = 2.5$, $D_u = D_v = D_w = 1.0$, and $\phi_0 = 0.000\,5$.

where $H(x)$ is the Heaviside function $H(x) = 1$ ($x \geqslant 0$), 0 ($x < 0$). The center of the irradiation $x_{\text{irrad}}(t)$ in (2) is changed according to the aforementioned relation $x_{\text{irrad}}(t) = x_{\text{front}}(t) + dev$, with the distance dev being kept constant throughout the irradiation. Note that the pulse front $x_{\text{front}}(t)$ can no longer be defined if the pulse solution collapses below the threshold v_{th}. In that case, the irradiation is stopped once $\max_{x\in\mathbf{R}} v(x,t) \leqslant v_{th}$.

The pulse width $\chi_0(t) = x_{\text{front}}(t) - x_{\text{back}}(t)$ serves as a criterion for the smallness of the irradiation width. In the next section, we numerically solve (1) with (2) to investigate the influence of the local comoving irradiation, whose width is sufficiently small compared to the pulse width.

III. NUMERICAL DETECTION OF ACHILLES' HEEL

In this section, we numerically investigate the behavior of the stable traveling pulse in (1) under the local comoving irradiation in (2). For the moment, the irradiation width d_{irrad} is fixed at some small value, and the intensity ϵ_{irrad} and the deviation dev of the irradiation from the pulse front are varied. However, we also decrease the value of d_{irrad} later to see the dependence on the irradiation width.

A. Phase diagram for pulse dynamics

Before applying irradiation, we look at the case of no irradiation $\epsilon_{\text{irrad}} = 0$ (i.e., $\phi(x,t) \equiv \phi_0$). In this case, a stable traveling pulse solution is numerically observed for (1) under appropriate parameter values, as shown in Fig. 2(a). From the figure, we soon notice that the w component takes large values compared to the u and v components, which is presumably due to the smallness of the parameter ϵ_2. Furthermore, we also see that each of the u and v components takes one maximum and decays monotonically to the steady state, while the w component does not decay monotonically but forms a dent around the pulse front. From the profile of the v component, the threshold v_{th} and the pulse width χ_0 for the v component are determined as $v_{th} = 0.01274$ and $\chi_0 = 15.6$, respectively.

Next, let us consider the case where the traveling pulse is stimulated by the comoving local irradiation. As initial conditions, we take the stable traveling pulse for $\phi(x,t) \equiv \phi_0$ and apply the irradiation according to (2). Here, the irradiation width is taken to be $d_{\text{irrad}} = 1.0$, which is less than 7% of the pulse width for the v component before the irradiation. Once the irradiation is turned on, the traveling pulse begins to shrink and slow down, since the positive value of $\phi(x,t)$ in (1) leads to the increase in the inhibitor w. When the irradiation strength ϵ_{irrad} is not very large, the traveling pulse endures the

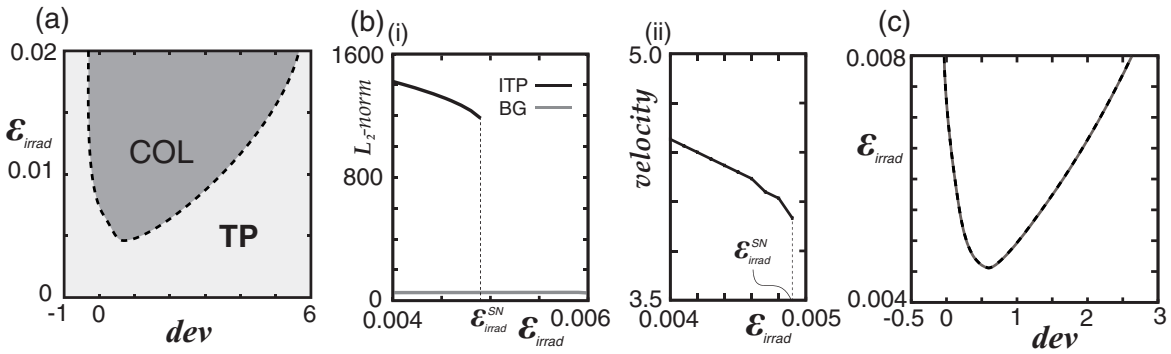

FIG. 3. (a) The phase diagram for the pulse behavior obtained numerically for (1) with (2). The irradiation width is $d_{\mathrm{irrad}} = 1.0$. The horizontal and vertical axes denote the deviation of the irradiation center from the pulse front dev, and the irradiation intensity $\epsilon_{\mathrm{irrad}}$, respectively. A stable traveling pulse is observed in the TP regime, while the traveling pulse eventually collapses for the parameters in the COL regime. (b) (i) The existence of the irradiated traveling pulse solution (black solid) and the spatially uniform solution (gray solid) obtained by numerical simulation for (1) with (2). The deviation dev is fixed at $dev = 1.0$, and the irradiation intensity $\epsilon_{\mathrm{irrad}}$ is varied. The vertical axis denotes the L_2 norm $\sqrt{\int_0^L \{u(x,t)^2 + v(x,t)^2 + w(x,t)^2\}\,dx}$ of a solution, where $L = 200$ is the system size for the numerical simulation. The stable irradiated traveling pulse (ITP) solution branch terminates at $\epsilon_{\mathrm{irrad}} = \epsilon_{\mathrm{irrad}}^{SN}$, while the spatially uniform solution (BG) is observed stably for the range of $\epsilon_{\mathrm{irrad}}$ we are concerned with. (ii) The ITP solution obtained by numerical simulation for (1) with (2). The deviation dev is fixed at $dev = 1.0$, and the irradiation intensity $\epsilon_{\mathrm{irrad}}$ is varied. (c) A saddle-node bifurcation curve (gray solid) obtained by changing the value of dev and plotting the saddle-node point $\epsilon_{\mathrm{irrad}}^{SN}$ in (b-i). The black dashed curve, which almost coincides with the gray solid curve, represents the TP-COL phase boundary in (a) magnified around the local minimum. Note that the saddle-node point $\epsilon_{\mathrm{irrad}}^{SN}$ in (b-i), and hence the saddle-node bifurcation curve, was obtained by increasing the value of $\epsilon_{\mathrm{irrad}}$ and continuating the ITP solution, while the TP-COL boundary in (a) was obtained by the direct numerical simulation for each dev and $\epsilon_{\mathrm{irrad}}$, with the initial condition fixed as the traveling pulse before the irradiation shown in Fig. 2(a). The parameters are the same as those in Fig. 2.

irradiation and asymptotes to another stable traveling pulse solution which propagates with constant shape and velocity, which differs from the original values [Fig. 2(b)]. The velocity of the traveling pulse decreases monotonically with $\epsilon_{\mathrm{irrad}}$ [Fig. 3(b-ii)]. The pulse shape shrinks as a whole compared to that before the irradiation in (a), but the w component locally takes a large value in the irradiated part. Hereafter, we call the stable traveling pulse solution under the comoving irradiation an irradiated traveling pulse (ITP). For a relatively large $\epsilon_{\mathrm{irrad}}$, on the other hand, the pulse can no longer hold its shape and eventually collapses to a spatially uniform solution. Thus, we find that the pulse either travels on (TP) or collapses (COL) in response to the irradiation, obtaining a phase diagram by varying the two parameters dev and $\epsilon_{\mathrm{irrad}}$ [Fig. 3(a)]. We found, however, that the value of $\epsilon_{\mathrm{irrad}}$ necessary for the pulse collapse varies depending on dev, such that the phase boundary is convex-downward. In particular, the phase boundary has a local minimum, indicating a special point in the traveling pulse at which it collapses with the lowest irradiation intensity. Hereafter, such a point in the pulse corresponding to the local minimum is called the Achilles' heel of the traveling pulse.

The phase diagram also suggests a bifurcation involved in the TP-COL transition as the parameters are varied, which is explained as follows: When dev is fixed and $\epsilon_{\mathrm{irrad}}$ is increased from below, it is found that an ITP solution ceases to exist at a value denoted by $\epsilon_{\mathrm{irrad}}^{SN}$, indicating a saddle-node bifurcation of the traveling pulse solution [Fig. 3(b-i)]. By plotting the saddle-node point with the variation of dev, we obtain a saddle-node bifurcation curve [Fig. 3(c)], which fits quite well with the TP-COL phase boundary in Fig. 3(a). This finding provides numerical evidence that the TP-COL transition is caused by a saddle-node bifurcation of the ITP solution, at least for the parameters near the local minimum of the phase boundary. Also note that a stable spatially uniform solution coexists with the ITP solution for $\epsilon_{\mathrm{irrad}} \leqslant \epsilon_{\mathrm{irrad}}^{SN}$. After the irradiation is switched on at $t = t_{\mathrm{irrad}}$, however, the initial stable traveling pulse solution for $\epsilon_{\mathrm{irrad}} = 0$ does not converge to the uniform solution but rather to an ITP solution, as long as there is a stable ITP solution.

B. Location of Achilles' heel

In the previous section, we fixed the irradiation width d_{irrad} and found that there was a special point in the traveling pulse solution where it collapsed with the lowest irradiation intensity. In order to identify the Achilles' heel of the traveling pulse more precisely, the irradiation width should be as small as possible.

Figure 4(a-i) shows the phase boundaries of the TP-COL transition for the smaller widths of $d_{\mathrm{irrad}} = 1.0$, 0.5, and 0.25. We realize that a higher intensity is needed for the collapse of the traveling pulse as the width becomes smaller. However, the values of dev for the local minima of the phase boundaries remain approximately unchanged for different values of d_{irrad}, which seem to fall in the range of $dev \in [0.3, 0.4]$ [Figs. 4(b-i) and 4(c-i)]. Considering that dev denotes the distance between the pulse front and the center of the irradiation, the aforementioned range of dev corresponds to a part of the pulse profile in Fig. 2 near the edge of the dent of the w component and a little ahead of the localized excited region of the u and v components [Fig. 4(a-ii)].

Furthermore, if the product $d_{\mathrm{irrad}} \times \epsilon_{\mathrm{irrad}}$ is used instead of $\epsilon_{\mathrm{irrad}}$, the lowest intensity for the collapse seems to converge to a value of about 0.004 as the width is decreased [Figs. 4(b-ii)

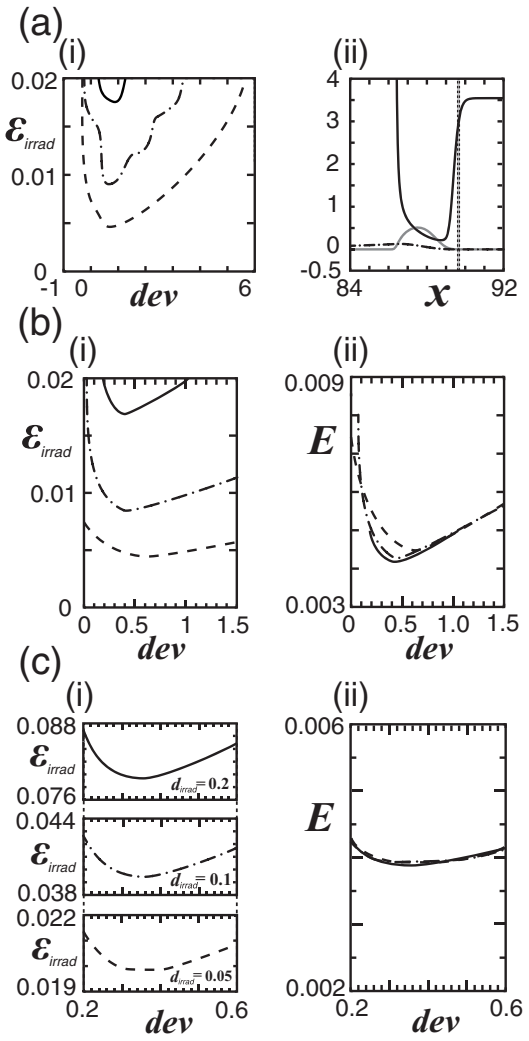

FIG. 4. (a) (i) The TP-COL phase boundaries obtained numerically for (1) with (2) for the three different irradiation widths of $d_{\text{irrad}} = 1.0, 0.5$, and 0.25, which are represented by the dashed, dash-dot, and solid curves, respectively. (ii) A magnification of the profile of the stable traveling pulse solution in Fig. 2. The vertical shaded region denotes the range $dev \in [0.3,0.4]$. (b) (i) The magnified phase boundaries of Fig. 4(a-i) around the local minima. (ii) The three phase boundaries in (i) plotted with the vertical axis replaced by $E = d_{\text{irrad}} \times \epsilon_{\text{irrad}}$. (c) (i) The TP-COL phase boundaries obtained numerically for (1) with (2) for the three different irradiation widths of $d_{\text{irrad}} = 0.2, 0.1$, and 0.05, which are represented by the dashed, dash-dot, and solid curves, respectively. (ii) The three phase boundaries in (i) plotted with the vertical axis replaced by $E = d_{\text{irrad}} \times \epsilon_{\text{irrad}}$. The other parameters are the same as those in Fig. 2.

and 4(c-ii)]. From (1) and (2), we see that the quantity $E = d_{\text{irrad}} \times \epsilon_{\text{irrad}}$ may be regarded as a kind of irradiation energy pumped in per unit time to the w component, which suggests that the lowest "energy" for the collapse of the traveling pulse remains the same for sufficiently small irradiation widths. Also note that the limit $d_{\text{irrad}} \to 0$ with E constant is equivalent to considering a sequence of functions that converge to the δ function. Together with the smallness of the irradiation width d_{irrad} in comparison to the pulse width, these numerical observations lead us to conjecture that, as $d_{\text{irrad}} \to 0$, the values of dev and E for the local minimum converge to $dev^* \in [0.3,0.4]$ and $E^* \in [0.003,0.004]$, respectively, which correspond to the location and the minimal irradiation energy for the collapse of the Achilles' heel, respectively.

IV. EXPERIMENTS

As mentioned at the beginning of Sec. II, the Oregonator was proposed as a model system for the chemical reaction called the Belousov-Zhabotinsky reaction [14]. We conducted experiments using a photosensitive BZ medium [26,27] in order to validate the numerical predictions.

A. Experimental setup

$Ru(bpy)_3Cl_2$, which was used as a catalyst for the photosensitive BZ reaction, was purchased from Sigma-Aldrich (St. Louis, MO). $NaBrO_3$ and H_2SO_4 were purchased from Nacalai Tesque, Inc. (Kyoto, Japan), and KBr and malonic acid $CH_2(COOH)_2$ were purchased from Wako Pure Chemicals (Osaka, Japan). The final concentrations of the BZ medium were $[NaBrO_3] = 0.53$ M, $[H_2SO_4] = 0.29$ M, $[CH_2(COOH)_2] = 0.15$ M, $[KBr] = 0.01$ M, and $[Ru(bpy)_3Cl_2] = 1.7$ mM. A cellulose nitrate membrane filter (Advantec, A100A025A, diameter of the membrane = 25 mm, thickness = 150 μm) with a pore size of 1 μm was immersed in the BZ medium, as described in our previous papers [28,31,42,54]. The experiments were performed in an air-conditioned room at 300 ± 2 K.

The experimental setup for light irradiation of the BZ medium, the monitoring system, and the image analysis was similar to those in previous studies, as shown schematically in Fig. 5 [28,31,42,54]. The high-pressure mercury bulb of a liquid-crystal projector (Mitsubishi, LPV-XL8) was used as a light source. The experimental field was composed of three regions: the excitable region where a chemical wave could propagate but could not be initiated without stimulation, the outer inhibitory region where a chemical wave could neither be generated nor propagate, and the oscillatory region as a source to induce a chemical wave in the excitable region. The light intensities for the excitable and inhibitory regions were constant at $\epsilon_0 = 5.2$ klx and $\epsilon_{\text{out}} = 64.3$ klx. A chemical wave was generated at the edge of the oscillatory region with a triangular shape and propagated towards the excitable region with a rectangular shape. The half-width of the chemical wave, which corresponded to the case of $v_{th} = v_{\max}/2$ according to the notation in Sec. II, was measured from the wave profile to be $\chi_0 = 0.46$ mm. A light pulse was irradiated in a rectangular area inside the excitable region. The width of pulse irradiation was set to be $d_{\text{irrad}} = 0.45$ mm. The light intensity at the irradiated region was measured with a light intensity meter (As-one, LX-100). The motion of a chemical wave was detected by the system consisting of a digital video camera (Sony, DCR-PC120) and a personal computer (Dell, Latitude D531), and the light pulse was irradiated instantly according to the position of the chemical wave detected. The spatial profile of the light intensity was determined by changing the gray level on the personal computer. This feedback system enabled us to move the irradiation area together with a chemical

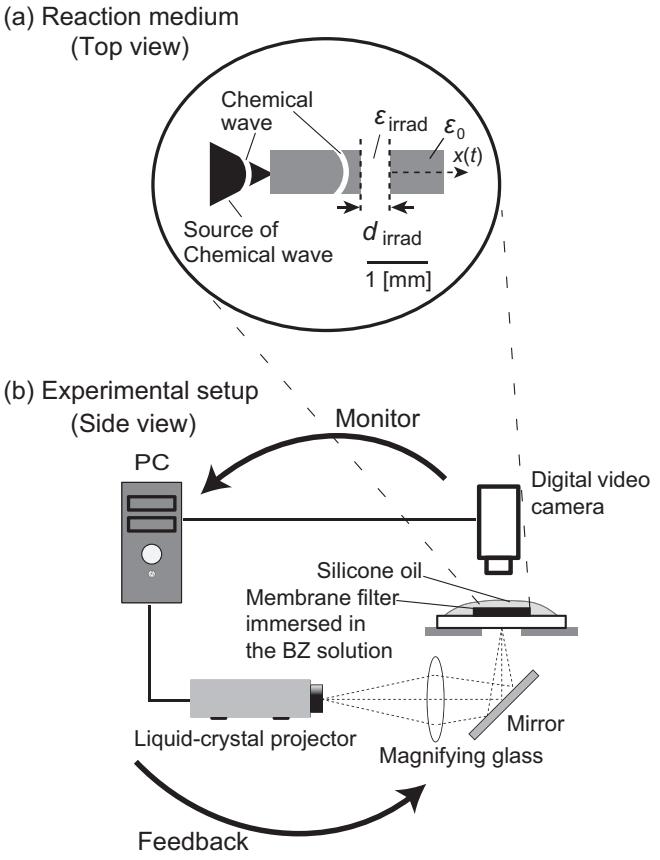

FIG. 5. Schematic illustration of (a) the reaction medium (top view) and (b) the experimental setup (side view).

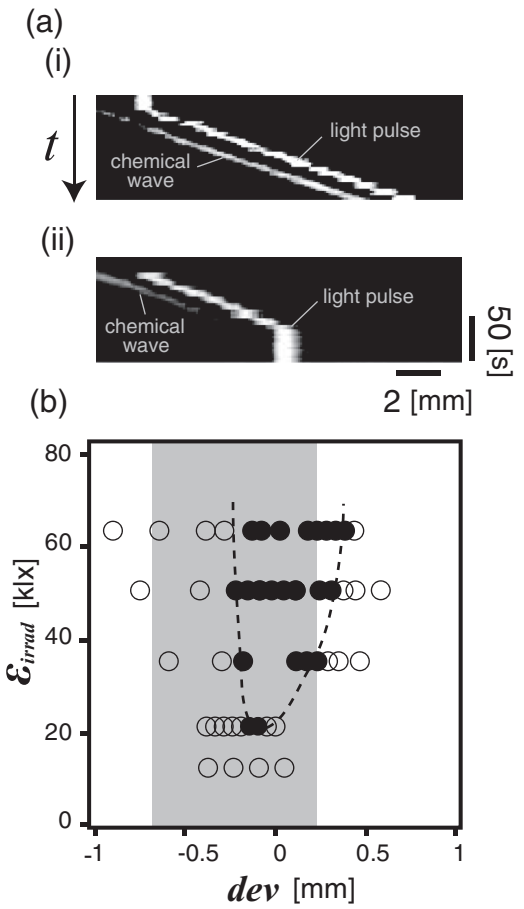

FIG. 6. (a) Experimental results for the propagation of a chemical wave for different values of dev: (i) traveling pulse, $\epsilon_{\text{irrad}} = 51.5$ klx, and $dev = 0.59$ mm; (ii) collapse, $\epsilon_{\text{irrad}} = 51.5$ klx and $dev = 0.25$ mm. The horizontal and vertical axes denote space and time, respectively. The analyzed region was along the x axis, as defined schematically in Fig. 5. (b) Experimental results for ϵ_{irrad} depending on dev for light pulse irradiation to a chemical wave. The collapse and the traveling pulse are shown by filled and empty circles, respectively. d_{irrad} was fixed at 0.45 mm. The shaded region $-0.69 < dev < 0.23$ corresponds to the range in which the light pulse completely or partly overlapped a chemical wave. An estimated boundary is also superposed with the dashed curve to facilitate comparison with the numerical counterpart in Fig. 3(a).

wave, keeping the distance between the irradiation and the chemical wave roughly constant. d_{irrad} and ϵ_{irrad} were changed individually.

B. Experimental results

Figure 6(a) shows the space-time diagrams for the propagation of a chemical wave obtained experimentally for (i) $dev = 0.59$ mm and (ii) $dev = 0.25$ mm. d_{irrad} and ϵ_{irrad} were 0.45 mm and 51.5 klx, respectively. The chemical wave propagated with nearly the same speed as the irradiated area and kept propagating for (i) [Fig. 6(a-i)], but the chemical wave collapsed for (ii) [Fig. 6(a-ii)].

In the experiments, the collapse of a chemical wave was observed under a local irradiation when the irradiation region overlapped the wave, as shown by the shaded region in Fig. 6(b), but it also collapsed when the irradiated region was a little distance away from the wave.

V. DISCUSSION

Although the collapse of a chemical wave was also observed in the experiments, a sensitive point was not seen as clearly as in the numerical simulations. This is partly because the irradiation width was almost as large as the wave.

On the other hand, numerical simulations with small irradiation width clarified the detailed position of the sensitive point in relation to the profile of the traveling pulse solution. As Fig. 2(a) shows, the traveling pulse solution has a characteristic dent in the w component around the pulse front, while the u and v components are localized around the bottom of the dent. From (1), we see that the irradiation leads to a local increase in the w component, which is directly reflected in the pulse profile [Fig. 2(b)]. In practice, the three components monotonically diminish in size after the irradiation is switched on, but the w component is locally increased, forming a bulge around the irradiated region. Upon collapse, the bulge grows further and the width of the dent becomes smaller until the dent bottom goes up, and the u and v components simultaneously decay to the background solution. Thus, the manner of deformation in the w component around the dent plays a key role in understanding the collapse of the pulse as a whole. Taking a closer look, we find that the profile of the w component

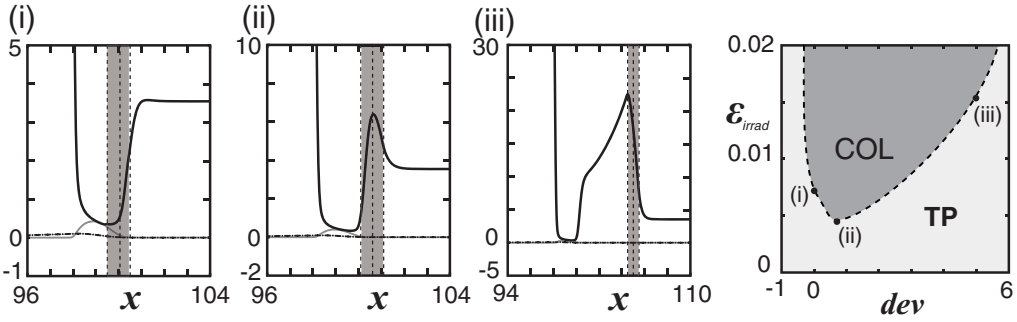

FIG. 7. The profiles of irradiated traveling pulse solutions observed numerically for $d_{\mathrm{irrad}} = 1.0$ and (i) $dev = 0.0$, (ii) $dev = 0.6$, and (iii) $dev = 5.0$. The parameters correspond to the three points in the TP regime labeled (i)–(iii) in the rightmost phase diagram, which is the same one as in Fig. 3(a). The u, v, and w components are represented by gray solid, dot-dash, and black solid curves, respectively. The w component of the profile is largely deformed for (ii) and (iii) around the irradiated part indicated by the shaded regions. The other parameters are given in Fig. 2.

under the irradiation differs depending on the value of dev (Fig. 7). When the pulse is irradiated near the Achilles' heel, the bulge is formed around the dent edge [Fig. 7(b-ii)]. The bulge is also formed when the pulse is irradiated to the right of the Achilles' heel [Fig. 7(b-iii)]. In this case, the w component is largest in the irradiated region and decreases as its distance away from the irradiated region increases, owing to the local reaction and diffusion. Therefore the value of w is smaller around the dent edge compared to the bulge peak. In contrast, the bulge is much less pronounced when the irradiation center is to the left of the Achilles' heel [Fig. 7(b-i)]. This observation implies that irradiation around the Achilles' heel induces the w component to deform most around the dent, with the dent becoming smaller; hence the pulse collapses with the least irradiation intensity.

We also tried similar simulations for the two-component reaction-diffusion system with modified Oregonator kinetics, which is also utilized as a model system for the photosensitive BZ reaction [32,35]. However, we confirmed that, unlike in the case of the three-variable one, a strongly irradiated part of the pulse collapsed to form a hump in the profile of the v component, rendering the position of the pulse front undefined and hence the location of the Achilles' heel unidentified. Therefore we may have to reconsider the definition of an interface for such cases of hump formation.

VI. CONCLUDING REMARKS

In this paper, we numerically studied the effect of a comoving local irradiation on a traveling pulse arising in the three-component reaction-diffusion system with modified Oregonator kinetics. From the numerical simulations, we found that the traveling pulse collapsed under a local irradiation of sufficiently high intensity, and whether the traveling pulse survived or collapsed depended on the part of the pulse irradiated. Qualitative features of the numerical results were also reproduced experimentally using the photosensitive BZ reaction.

For the numerical simulations, the irradiation width was considered to be sufficiently small compared to the pulse size. This allowed us not only to suggest the existence of the Achilles' heel, the most sensitive point in the traveling pulse, but also to discover that the energylike quantity of the irradiation remained nearly constant for smaller irradiation width. However, it is hard to further narrow down the irradiation width due to numerical limitations. In order to overcome this difficulty, the problem should be addressed analytically. For instance, Dockery *et al.* [56] and Kessler and Levine [57,58] analytically studied the stability of a traveling pulse solution using the Oregonator system with nonlinear terms of piecewise-linear type. Applying their methods, we may be able to explore the case of an infinitesimally small irradiation width, as well as to elucidate the factor that determines the location of the Achilles' heel.

For instance, spiral waves are observed in several biological, physical, and chemical systems. However, spiral waves in the heart of a living organism cause life-threatening tachyarrhythmia and ventricular fibrillation. Although antitachycardia pacing and cardioversion are currently in practical use for eliminating these undesired spiral waves, such treatments have serious drawbacks, and alternative methods were proposed recently [45,46,52,59]. If sensitive points are also found for two-dimensional patterns including spiral waves, they may be eliminated efficiently by tracing the wave front and giving pinpoint stimuli, which, in the future, may lead to a method complementary to the aforementioned methods.

ACKNOWLEDGMENTS

This work was supported in part by JSPS KAKENHI through Grants No. 26247015, No. 25410094, and No. 16H03949 and JSPS A3 Foresight Program. The authors thank Masaharu Nagayama (Hokkaido University, Japan) for valuable comments.

[1] J. M. Davidenko, P. Kent, and J. Jalife, Physica D **49**, 182 (1991).
[2] J. M. Davidenko, A. V. Pertsov, R. Salomontsz, W. Baxter, and J. Jalife, Nature (London) **355**, 349 (1992).
[3] A. L. Hodgkin and A. F. Huxley, J. Physiol. **117**, 500 (1952).
[4] K. S. Cole and H. J. Curtis, J. Gen. Physiol. **22**, 649 (1939).
[5] N. A. Gorelova and J. Bureš, J. Neuro. Biol. **14**, 353 (1983).

[6] M. A. Dahlem and S. C. Müller, Exp. Brain Res. **115**, 319 (1997).
[7] F. Siegert and C. J. Weijer, Proc. Natl. Acad. Sci. USA **89**, 6433 (1992).
[8] E. Pálsson and E. C. Cox, Proc. Natl. Acad. Sci. USA **93**, 1151 (1996).
[9] Y. A. Astrov, I. Müller, E. Ammelt, and H.-G. Purwins, Phys. Rev. Lett. **80**, 5341 (1998).
[10] E. Ammelt, Y. A. Astrov, and H.-G. Purwins, Phys. Rev. E **55**, 6731 (1997).
[11] H. H. Rotermund, W. Engel, M. Kordesch, and G. Ertl, Nature (London) **343**, 355 (1990).
[12] J. J. Tyson and J. P. Keener, Physica D **32**, 327 (1988).
[13] E. Meron, Phys. Rep. **218**, 1 (1992).
[14] A. M. Zhabotinsky, M. D. Eager, and I. R. Epstein, Phys. Rev. Lett. **71**, 1526 (1993).
[15] M. D. Graham, I. G. Kevrekidis, K. Asakura, J. Lauterbach, K. Krischer, H.-H. Rotermund, and G. Ertl, Science **264**, 80 (1994).
[16] M. Bär, A. K. Bangia, I. G. Kevrekidis, G. Haas, H.-H. Rotermund, and G. Ertl, J. Phys. Chem. **100**, 19106 (1996).
[17] M. Bär, E. Meron, and C. Utzny, Chaos **12**, 204 (2002).
[18] A. Kulka, M. Bode, and H.-G. Purwins, Phys. Lett. A **203**, 33 (1995).
[19] N. Manz, V. A. Davydov, V. S. Zykov, and S. C. Müller, Phys. Rev. E **66**, 036207 (2002).
[20] R. R. Aliev and A. B. Rovinskii, J. Phys. Chem. **96**, 732 (1992).
[21] O. Steinbock, V. Zykov, and S. C. Müller, Nature (London) **366**, 322 (1993).
[22] S. Grill, V. S. Zykov, and S. C. Müller, Phys. Rev. Lett. **75**, 3368 (1995).
[23] V. Petrov, Q. Ouyang, and H. L. Swinney, Nature (London) **388**, 655 (1997).
[24] M. Dolnik, I. Berenstein, A. M. Zhabotinsky, and I. R. Epstein, Phys. Rev. Lett. **87**, 238301 (2001).
[25] L. B. Smolka, B. Marts, and A. L. Lin, Phys. Rev. E **72**, 056205 (2005).
[26] L. Kuhnert, Naturwissenschaften **73**, 96 (1986).
[27] L. Kuhnert, Nature (London) **319**, 393 (1986).
[28] S. Nakata, T. Ezaki, Y. S. Ikura, and H. Kitahata, J. Phys. Chem. A **117**, 10615 (2013).
[29] A. P. Muñuzuri, V. Pérez-Villar, and M. Markus, Phys. Rev. Lett. **79**, 1941 (1997).
[30] R. Tóth, V. Gáspár, A. Belmonte, M. C. O'Connell, A. Taylor, and S. K. Scott, Phys. Chem. Chem. Phys. **2**, 413 (2000).
[31] S. Nakata, M. Matsushita, T. Sato, N. J. Suematsu, H. Kitahata, T. Amemiya, and Y. Mori, J. Phys. Chem. A **115**, 7406 (2011).
[32] M. Tanaka, H. Nagahara, H. Kitahata, V. Krinsky, K. Agladze, and K. Yoshikawa, Phys. Rev. E **76**, 016205 (2007).
[33] K. Agladze, Á. Tóth, T. Ichino, and K. Yoshikawa, J. Phys. Chem. A **104**, 6677 (2000).
[34] H. Kitahata, R. Aihara, Y. Mori, and K. Yoshikawa, J. Phys. Chem. B **108**, 18956 (2004).
[35] J. Miyazaki and S. Kinoshita, Phys. Rev. E **76**, 066201 (2007).
[36] Y. Nishiura, T. Teramoto, and X. Yuan, Comm. Pure Appl. Anal. **11**, 307 (2012).
[37] Y. Nishiura, T. Teramoto, X. Yuan, and K.-I. Ueda, Chaos **17**, 037104 (2007).
[38] M. Bär, A. Hagberg, E. Meron, and U. Thiele, Phys. Rev. E **62**, 366 (2000).
[39] V. A. Davydov, N. Manz, O. Steinbock, V. S. Zykov, and S. C. Müller, Phys. Rev. Lett. **85**, 868 (2000).
[40] H. Ikeda and S.-I. Ei, Physica D **239**, 1637 (2010).
[41] A. Hagberg and E. Meron, Phys. Rev. E **57**, 299 (1998).
[42] T. Ichino, K. Fujio, M. Matsushita, and S. Nakata, J. Phys. Chem. A **113**, 2304 (2009).
[43] H. Sevčíková, M. Marek, and S. C. Müller, Science **257**, 951 (1992).
[44] T. Sakurai, E. Mihaliuk, F. Chirila, and K. Showalter, Science **296**, 2009 (2002).
[45] M. Tanaka, A. Isomura, M. Hörning, H. Kitahata, K. Agladze, and K. Yoshikawa, Chaos **19**, 043114 (2009).
[46] A. Isomura, M. Hörning, K. Agladze, and K. Yoshikawa, Phys. Rev. E **78**, 066216 (2008).
[47] S. Kitawaki, K. Shioiri, T. Sakurai, and H. Kitahata, J. Phys. Chem. C **116**, 26805 (2012).
[48] Á. Tóth and K. Showalter, J. Chem. Phys. **103**, 2058 (1995).
[49] O. Steinbock, P. Kettunen, and K. Showalter, J. Phys. Chem. **100**, 18970 (1996).
[50] Á. Tóth, D. Horváth, and K. Yoshikawa, Chem. Phys. Lett. **345**, 471 (2001).
[51] O. Steinbock, Á. Tóth, and K. Showalter, Science **267**, 868 (1995).
[52] A. Pumir, V. Nikolski, M. Hörning, A. Isomura, K. Agladze, K. Yoshikawa, R. Gilmour, E. Bodenschatz, and V. Krinsky, Phys. Rev. Lett. **99**, 208101 (2007).
[53] A. V. Panfilov, S. C. Müller, V. S. Zykov, and J. P. Keener, Phys. Rev. E **61**, 4644 (2000).
[54] S. Nakata, S. Suzuki, T. Ezaki, H. Kitahata, K. Nishi, and Y. Nishiura, Phys. Chem. Chem. Phys. **17**, 9148 (2015).
[55] H.-J. Krug, L. Pohlmann, and L. Kunert, J. Phys. Chem. **94**, 4862 (1990).
[56] J. D. Dockery, J. P. Keener, and J. J. Tyson, Physica D **30**, 177 (1988).
[57] D. A. Kessler and H. Levine, Physica D **39**, 1 (1989).
[58] D. A. Kessler and H. Levine, Phys. Rev. A **41**, 5418 (1990).
[59] S. Takagi, A. Pumir, D. Pazó, I. Efimov, V. Nikolski, and V. Krinsky, J. Theor. Biol. **230**, 489 (2004).